Preliminary Observations of the Sequence of Damage in Excised Human Juvenile Cranial Bone at Speeds Equivalent to Falls from 1.6 m

Tom Brooks[1], Johann Zwirner[2], Niels Hammer[3,4,5], Benjamin Ondruschka[6], Mark Jermy[1*]

[1] Department of Mechanical Engineering, University of Canterbury, Christchurch, New Zealand

[2] Department of Anatomy, University of Otago, Dunedin, New Zealand

[3] Medical University of Graz, Department of Macroscopic and Clinical Anatomy, Graz, Austria

[4] Department of Orthopedic and Trauma Surgery, University of Leipzig, Leipzig, Germany

[5] Fraunhofer IWU, Dresden, Germany

[6] Institute of Legal Medicine, University Medical Center Hamburg-Eppendorf, Hamburg, Germany

*Corresponding Author, mark.jermy@canterbury.ac.nz

Tom Brooks and Johann Zwirner are young researchers.

Abstract

There is much debate within the forensic community around the indications that suggest a head injury sustained by a child resulted from abusive head trauma, rather than from accidental causes, especially when a fall from low height is the explanation given by a caregiver. To better understand this problem, finite element models of the paediatric head have been and continue to be developed. These models require material models that fit the behaviour of paediatric head tissues under dynamic loading conditions. Currently, the highest loading rate for which skull data exists is 2.81 ms^{-1}. This study improves on this by providing preliminary experimental data for a loading rate of 5.65 ± 0.14 ms^{-1}, equivalent to a fall of 1.6 m. Eleven specimens of paediatric cranial bone (frontal, occipital, parietal and temporal) from seven donors (age range 3 weeks – 18 years) were tested in three-point bending with an impactor of radius 2 mm. It was found that prompt brittle fracture with virtually no bending occurring in all specimens but those aged 3 weeks old, where bending preceded brittle fracture. The maximum impact force increased with age (or thickness) and was higher in occipital bone. Energy absorbed to failure followed a similar trend, with values 0.11 and 0.35 mJ/mm^3 for age three-weeks, agreeing with previously published static tests, increasing with age up to 9 mJ/mm^3 for 18-year-old occipital bone. The preliminary data provided here can help analysts improve pediatric head finite element models that can be used to provide better predictions of the nature of head injuries from both a biomechanical and forensic point of view.

Keywords pediatric, children, impact, biomechanics, head injury

Declarations

Funding: T Brooks is the recipient of a University of Canterbury Doctoral Scholarship

Conflicts of interest: None

Availability of data and material: data is available on request to the authors

Code availability: No relevant code was used in the preparation of this work

Acknowledgements

The authors would like to thank Dr Marzi Anjomrouz from MARS Bioimaging Ltd for her help with the spectral CT imaging of the specimens.

Introduction

Domestic accidental falls are one of the most common items of anamnestic evidence offered by persons suspected of inflicting abusive head trauma (AHT) on children [1]. Plunkett [2] reviewed more than 75,000 cases involving head and neck injuries in children that were stated as resulting from the use of playground equipment and concluded that short distance falls may cause fatal paediatric head injuries. Some forensic pathologists disagree with this potential lethality and challenge the reliability of the witnesses. This is one of the most intensively discussed topics in clinical forensics, starting from one study by Chadwick et al. [3], who reviewed 317 cases of child injuries where the history was described by the caretaker as being that the child had fallen. In 100 cases where the child had fallen less than 1.2 m, seven were fatal, and in 117 cases of falls between three and 14 m, one was fatal. The seven fatalities in the short falls all had factors in their cases suggesting false histories [3]. If the histories of these seven cases were to be believed, the results indicate that the risk of fatal injuries increases with decreasing fall heights. Knowing this controversy, Johnson et al. [1] reviewed 72 cases of toddlers admitted to one Accident and Emergency department with head injuries resulting from reportedly accidental falls and concluded that typical accidental falls of less than one metre that occur in normal domestic situations do not commonly cause skull fractures. Hobbs [4] found that skull fractures that were a result of an accident were generally at only one localisation, presenting as narrow linear fractures that did not exceed skull sutures, and which were only rarely associated with intracranial injuries. However, AHT resulted in multiple, depressed and/or growing fractures along with intracranial injuries such as subdural hematoma (SDH), cortical concussions and diffuse axonal injuries (DAI). Similar results were also found by Chadwick et al. [3],Wilkins [5],Reece, Sege [6],Roach et al. [7] and Williams [8].

Although such injury indicators may point to a particular incident being *probably* a result of an accident or abuse, without reliable witnesses to the history of the injury – and AHT instances are unwitnessed in almost all cases from our own experience- it is not possible to be sure, or to quantify the probability when using only radiological data of the head. Therefore, research is in progress to develop ways to predict the injury pattern from different types of head impact [9-12]. Most of these studies use finite element (FE) methods to predict the propagation of mechanical stress and tissue damage. These methods rely on models of the mechanical response of tissues. Such models are based on mechanical response data, which is scarce for infant human head tissues at the strain rates encountered in injurious impacts. The purpose of the present study was to make preliminary observations for the very first time on how post-mortem human child cranial bone behaves at relatively higher impact velocities rather than in quasi-static conditions, to get the closest possible approach to real impacts.

The first studies on infant cranial bone acquired their data under static loading conditions [13,14]. McPherson, Kriewall [14] tested 83 samples of human infant cranial bone (gestational age range of 25 to 40 weeks) in three-point bending at a rate of 0.5 mm/min. Margulies, Thibault [13] also conducted three-point bend tests on 12 samples of human infant cranial bone (age range of 25 weeks gestation to six months) at loading rates of 2.54 and 2540 mm/min. Both studies investigated the elastic modulus as a function of age, with agreement between the two. Margulies, Thibault [13] also investigated the stress at fracture and energy absorbed to failure. Cranial bone data obtained under static loading conditions is limited for children up to 18 years. Wang et al. [15] conducted three-point bend testing on 56 samples of cranial bone and suture from one to two-year old children at a loading rate of 1.5 mms^{-1}. Davis et al. [16] conducted four-point bend tests on 47 samples of cranial bone from a six-year old child (average strain rates of 0.045, 0.44 and 2.2 s^{-1}). The only study to date that has investigated the rate dependence of the material properties for infant cranial bone is that of Coats, Margulies [17]. Coats, Margulies [17] conducted three-point bend impact testing on 46 infant skull bone samples at fall heights of 0.3 and 0.9 m, resulting in impact speeds of 1.58 and 2.81 ms^{-1} respectively. The published data on infant head tissue properties, up to 2018, is reviewed in [18]. Ommaya et al. [19] reviewed studies of the causative mechanisms of traumatic brain injury, and the effect of differences between adult and juvenile physiology. They noted that skull fracture severity correlates with age-dependent cranial bone thickness and state of the cranial sutures.

This paper reports high speed imaging observations on the behaviour of human infant bone in three-point bend impacts at a speed equivalent to a fall of up to 1.6 m. To the best of the authors' knowledge, there are no published studies that have conducted impact testing on infant or child cranial bone at speeds greater than that equivalent to 'higher than a one metre fall' or captured high-speed imagery of the impact. Observations of energy absorbed to failure, minimum fracture speed and maximum impact force are interpreted in terms of trends with average bone thickness, age and hydroxyapatite (HA) density and the cranial plate from which the sample was taken (frontal, occipital, parietal or temporal).

Methods

Specimen Preparation

Eleven specimens from seven cadavers were obtained from the Institute of Legal Medicine, University of Leipzig, Germany (ethics approval 486/16-ek). Donor ages ranged from three weeks to 18 years to fully display the age spectrum of pediatric samples from infants to teenagers.

Following the total removal of the soft tissues of the cranium, including the skin, periosteum externally and the dura mater internally, the specimens were sectioned into samples measuring approximately 10 by 20 mm. Following this, the samples were precooled at four degrees Celsius prior to shock freezing them for storage and transportation purposes. Prior to the experiments, the samples were thawed and sectioned into their final shape using a piezo surgery device (PIEZOSURGERY white, Mectron s.p.a, Genova, Italy). Table 1 lists the age, sex, dimensions and cranial bone localisation for each of the specimens used in the given study. All specimens of the same age are from the same donor.

The surface of the specimens were spray painted white and a speckle pattern was created by grinding pencil lead graphite into a sieve and sprinkling it over the face for digital image correlation (DIC) usage.

To determine the average thickness of the specimens, the thickness at each end and in the middle was measured using digital calipers.

Spectral Computed Tomography

Spectral CT [20] was used to image each specimen before the impacts were conducted so that each samples' mineral density could be measured using a MARS 10 (Medipix All Resolution System) scanner (MARS Bioimaging Ltd., Christchurch, New Zealand). Scan settings included an exposure time of 200 µs and a slice thickness of 80 µm, with a 1.96 mm thick aluminium filter. The specimens were mounted in a 3D printed capsule using Blu Tack (Bostik, Milwaukee, USA), as shown in Figure 1.

The geometry of the specimens was reconstructed using the MARS Vision software. A material decomposition (MD) analysis was carried out on the reconstructed images using the MARS-MD algorithm [21]. This created a set of images for each of HA, water (hydrophilic content) and lipid (lipophilic content) illustrating their concentrations.

The HA concentration was measured using a bone analysis code by Matanaghi et al. [22]. This code is a plugin for the ImageJ [23] distribution FIJI [24] and allows the cortical and cancellous layers of the bone to be segmented separately so as to be able to determine the density of each.

Impact Test Machine

Impact testing was carried out on a custom-built machine that consisted of a pneumatic cylinder controlled by a 5/3 solenoid valve with a switching time of 11 ms. A relatively fast switching time was important so that the high pressure side of the cylinder is vented to atmosphere once the impactor is up to speed. The low pressure side is permanently vented to the atmosphere. This allowed for minimal additional force on the impactor during the impact to maintain conservation of energy. A microcontroller was used to control the valve switch timing. Figure 2 shows the impact machine setup.

The specimens were placed on steel support beams in a three-point bending test setup. The support beams had a radius of one millimetre and could be rotated about the longitudinal axis to account for any irregularity in the lateral direction (out-of-plane) of the specimens. Due to the three-dimensional curvature of the specimens, there was no position in which there was continuous contact with the supports at each end of the specimen, hence the supports were not rotated for these tests. The lack of continuous end contact resulted in compression of the specimen onto the supports during the impact tests. This would have occurred regardless of the orientation of the supports used.

The impactor head had a radius of two millimetres. It was painted black with white tracking dots so that its speed could be measured from the image sequence.

High-Speed Imagery

Two SA5 cameras (Photron, Tokyo, Japan) were used to image the impact from the front and rear of the specimen (that is, perpendicular to the face of the impactor head). The cameras were synchronised so that their images were acquired simultaneously. The imaging settings are outlined in Table 2.

Impact velocity was measured in GOM Correlate Professional (GOM GmbH, Braunschweig, Germany) by tracking the white dots on the impactor head during the image sequence. Distances in the image were calibrated using the known dimensions of the impactor head. The displacement and acceleration of the impactor were also measured using GOM Correlate Professional.

The high-speed image sequences were used to calculate:

Impact force using the acceleration and mass of the impactor (0.572 ± 0.001 kg).

Energy Absorbed to Failure using the change in kinetic energy of the impactor and normalised with respect to the volume of the specimen. It was assumed that all the energy lost by the impactor was absorbed by the specimen. The change in the kinetic energy was based on the change in velocity of the impactor from when it first contacted the specimen to when the first osseous discontinuity appeared. First contact and first discontinuity were manually identified from the images.

Minimum Fracture Propagation Speed by measuring the distance the crack tip travelled between image frames. Distance was measured using the 'measure' function in the Photron FASTCAM Viewer (PFV) software [25]. The crack propagated through the thickness of the specimen in less than the time between image frames, so it was only possible to infer a lower bound on speed, here termed as the 'minimum'.

Results

Observations from High Speed Imaging

The sequence of events leading to the fracture of the specimens is similar across all samples. Figure 3 shows a typical series of images (here illustrated for the impact of specimen #6). Due to the curvature in the specimens, the ends of the specimen are not fully sitting on the support beams. This results in torsion within the sample as the impactor settles the edges onto the support beams. Within one frame (50 μs) of settling, prompt brittle fracture occurs. Very little bending (if at all) is observed at this frame rate.

A force-displacement plot for the impact of specimen #6 is shown in Figure 4. In the frame sequence, the plot data corresponds to frames two through to six (initial contact to fracture). As initial contact occurred between frames one and two, the initial displacement is not zero as expected, but rather, is the distance the impactor travelled between frames one and two. From frame two through to five, the force increases up to a maximum of approximately 3000 N. This corresponds to the point where the specimen is settling onto the supports and internal compression within the specimen is occurring and bending starts. The impact force halves within one frame, corresponding to the fracture that is observed as the bone fails.

The force-displacement plot of Figure 4 is typical of the impacts for the specimens where one or both ends were not able to fully sit on the supports. Where there was very little settling of the specimen onto the supports, fracture occurred within one or two frames of initial contact, after which force decreased as the fracture propagated.

The sequence of events leading to the failure in specimens #1 and #2 (three-weeks-old) were slightly different than the older specimens. Although all specimens were orientated so that they were loaded 'naturally' from outside to inside (the impactor head loads from the convex side), these very elastic three-weeks-old specimens bend and become concave on the loading side before fracture occurs. Figure 5 shows the sequence of events exemplified for specimen #2.

A force-displacement plot for the impact of specimen #2 is shown in Figure 6. As with Figure 4, the plot data corresponds to frames two through to six. The impact force increases from approximately 10 N up to a maximum of 140 N before fracture occurs. These forces are significantly less than those for specimen #6.

Average Thickness and HA Density vs Age

The average thickness increases linearly with age for each cranial bone (R^2=0.94, R^2=0.99 and R^2=0.79 for the frontal, occipital and parietal bone respectively), as shown in Figure 7(a). Only one data point

exists for the temporal bone, hence no regression line could be fitted. The logarithmic fit for all data points had R^2=0.81.

For each cranial bone, HA density varies linearly with age, as shown in Figure 7(b). Both the occipital and parietal bone show clear increases in HA density with age (R^2=0.98 and R^2=0.77 respectively for linear fits). However, the regression line for the frontal bone shows an approximate constant HA density with age. The logarithmic fit for all data points had R^2=0.84 and exceeded the linear fit of R^2=0.44.

Maximum Impact Force

Across all specimens, the maximum force on the impactor ranges from around 200 N through to approximately 6000 N (Figure 7(c)). The force measured in the occipital bone specimens (different individuals) is much greater than the other bone regions. For each cranial bone, the regression lines support a linear relationship with age (R^2=0.99, R^2=0.96, R^2=0.98 for frontal, occipital and parietal bone respectively).

Specimen #9 (boxed data point in Figure 7(c)) does not fit the general trend of increasing with age. Review of the high-speed imagery showed that the impactor was misaligned and impacted the specimen near the edge, close to the righthand support. This resulted in a small section of the specimen breaking off, and the fracture did not extend through the full thickness of the specimen. This would have resulted in the lower maximum impact force measured and therefore it was treated as an outlier and not used for generating the regression line.

Energy Absorbed to Failure

For each cranial bone, the energy absorbed to failure (normalised with respect to volume) increased with age (Figure 7(d)). Regression lines show a linear increase (R^2=0.85, R^2=0.87, R^2=0.92 for frontal, occipital and parietal bone respectively). The occipital bone absorbs the most energy before failure while it is the thickest here investigated calvarial segment. As with maximum impact force, specimen #9 was treated as an outlier (boxed data point in Figure 7(d)).

Minimum Fracture Propagation Speed

There were no observable trends for the minimum fracture speed in relation to age or average thickness (not shown graphically). Speeds ranging from 28 to 100 ms^{-1} were measured, however, these are the minimum speeds consistent with the data, and not necessarily the actual fracture speed due to limitations with the camera frame rate.

Discussion

This study is a preliminary investigation into the behaviour of infant and child cranial bone at impact velocities equivalent to falls greater than one metre (1.6 m) (under three-point bend loading conditions). Due to the scarcity of human child specimens, future experimental work needs to be designed rigorously to maximise the data that can be obtained. Although the experimental procedures can theoretically be tested on animal bone or surrogates, there is, to date, no satisfying substitute for human specimens in general and paediatric samples in detail, especially when information on the specimens (such as physical dimensions and estimated biomechanical properties) may not be available during the design process.

Limitations

As with many experimental studies involving human tissues, there are limitations to the data presented in this study. Such limitations include the number and physical size of samples, and the lack of surrounding tissues that are make up the human head.

The greatest limitation in this study is the size of the data set. Only eleven samples from seven donors were used. Although this sample size may not be representative to fully investigate the trends observed, it provides some important data as there is little published data on child cranial material properties to date. The physical size of the specimens ranged from 15 to 22 mm in span and seven to 12 mm in width, which are not representative of an intact skull, but are similar in size to the specimens used by [17].

Impact experiments were conducted on bare cranial bone, with all surrounding tissues removed. This limits the data to that of the cranial bone alone and cannot be used to infer how the cranial bone would behave in its correct anatomical context. The surrounding tissues will have some influence on how the cranial behaves during an impact. Scalp and suture tissues are much softer than the cranial bone and would likely absorb some energy, hence reducing the likelihood of skull fracture occurring. The presence of brain and CSF would also offer some resistance to the deformation of the cranial bone.

Due to the relatively small physical size of the specimens, the impactor head had to be small (radius of two millimetres). This does not represent the physical size of an impact surface likely to be experienced during a fall or weapon. Such a size is more representative of an edge, such as falling onto the edge of household furniture.

The frame rate was a limiting factor in capturing the deformation of the specimen during the impact before fracture occurred. Although high intensity lighting was used, more light was required so that a

faster camera frame rate could be used. This would have allowed for the use of DIC to measure displacement and strain, which in turn could be used to calculate elastic modulus and ultimate strength, as well as in parametric finite element models to improve material models.

The calculation of the energy absorbed to failure assumed that the kinetic energy lost by the impactor was transferred to the specimen. However, there is likely to be some energy dissipation due to the frictional contact between the impactor and specimen. Any frictional losses are likely to be similar in magnitude for each impact and therefore only affect the reported values. Any relationships observed will be the same and hence any losses were assumed to be negligible. There were also frictional losses where the shaft of the impactor was in contact with the pneumatic cylinder bushing. This affects the speed of the impactor, however, the relatively short distance over which the impactor-specimen contact took place means that any energy loss would be minimal. Although the air supply was shut off after 10 ms and the pneumatic cylinder simultaneously vented to atmosphere, the residual pressure in the cylinder accelerates the impactor until the pressure is equalised.

In specimen #4, zigzagged discontinuities were observed in the CT scans. The zigzag nature indicates it is likely to be the metopic suture, which is still not fully ossified in the given age. From closer inspection of the images, it does not appear that the impact fractures initiated at the site of the suture. However, it cannot be certain if the suture had any relevant effect on the test failure of the specimens.

Observations from High Speed Imagery

The mean (± standard deviation) impact velocity was 5.65 ± 0.14 ms^{-1}. This is equivalent to a fall of approximately 1.6 m and all specimens exhibited fracture at this speed. No observations during the impact process on infant cranial bone at this high loading rate have ever been published to our knowledge, with the highest speed in prior studies being 2.81 ms^{-1} [17].

Except for the two three-week-old specimens, all specimens had virtually no bending before brittle fracture occurred. Specimens #1 and #2 were more flexible than the other specimens as visible bending occurred before they fractured. This is consistent with previous literature where the infant skull has been found to be more compliant than a child or adult skull [13,26,27].

The stiffness of any beam theory for a simply supported beam is the product of the elastic modulus and the beam's second moment of area (a function of beam thickness). McPherson, Kriewall [14],Margulies, Thibault [13],and Coats, Margulies [17] showed that the elastic modulus of pediatric cranial bone increases with age. The present specimens show a consistent trend of thickness increasing with age. Therefore, in these specimens, both elastic modulus and second moment of area increases with age, hence it is expected that the older the specimen, the less flexible it is.

The prompt brittle fracture of specimens #3 to #11 is likely to be due to the relatively greater HA density. It is well established that HA density increases with age and that an increase in HA density increases the brittleness of bone [28]. In these samples, the fractures started at the bottom, with the crack tip propagating upwards towards the top. This is expected due to the highest tensile stresses occurring at the bottom surface. The fracture often zigzagged, especially where there were clear transitions from the cortical to cancellous layers (and vice versa). This is likely due to the difference in the osseous microstructure and hence material behaviour of the two types of bone.

Force-displacement data would ideally be used to calculate the elastic modulus of the various cranial bones tested. However, no deflections were captured in the images due to the fractures appearing within one frame of the specimens settling onto the supports. The displacement data was that of the impactor and largely a result of the specimens undergoing bending and torsion until both ends were on the support beams.

Average Thickness and HA Density

Delye et al. [29] measured cranial bone thickness using 181 CT scans of 187 patients, ranging from zero to 20 years of age. They found that there was a rapid increase in the skull bone thickness in the first year of life, with the rate of increase slowing during year two. The thickness continued to increase further up to the age of 20, but the rate of increase slows substantially. A logarithmic relationship was determined for the skull thickness as a function of age. The data presented here fits the general trends found by Delye et al. [29], with magnitudes within one standard deviation of their mean values. Linear increases with age were identified for each cranial bone in this given study. A logarithmic curve fit was carried out for all data points to compare with Delye et al. [29]. The present data does not have enough points to determine whether a logarithmic or linear relationship fits the data better. Delye et al. [29] found no differences in thickness between male and female and our own autopsy experience show only negligible overall differences in cohorts of hundreds of cadavers, therefore differences in sex were not considered in this study.

Delye et al. [29] found a similar trend for the general increase in HA density with age as that for the skull thickness (logarithmic relationship). However, there was a steep increase in the density at the age of six years, reaching a peak at seven before dropping quickly at eight and returning to the general increase at age nine. When considering all data points in the present study, a logarithmic fit better represents the data than a linear fit, similar to that found by Delye et al. [29]. Due to no specimens being in the age range of five to 10 years, the sudden increase in density from ages six to eight cannot be tested with our data. The higher R^2 values for the linear relationships found for individual cranial bones is most likely due to the very small number of data points for each region. This is most apparent

for the frontal bone where the constant HA density with increasing age is unexpected based on the findings of Delye et al. [29].

Maximum Impact Force

Although maximum force data is not presented in the three or four-point bend test studies of Margulies, Thibault [13],Coats, Margulies [17],and Davis et al. [16], it can be inferred from the specifications of the load cells used that the maximum force did not exceed 250 N. A force-displacement plot presented by Coats, Margulies [17] shows that a maximum force of around 7 N was measured for static three-point bending of a parietal bone from a two month old donor. The maximum forces experienced by the three-week-old specimens in the present study were approximately 140 N (parietal) and 240 N (occipital). Without specific data to compare too, these magnitudes are higher than that of the similar age group in Margulies, Thibault [13],and Coats, Margulies [17]. This is expected due to the higher impact velocity.

In the data presented here, the maximum impact force ranges from approximately 200 N up to 6000 N. As there is limited data for human cranial bone up to 18 years in the literature, and that no previous studies exist for similar impact speeds, it cannot be determined if these magnitudes are to be expected. Given that the scalp, periosteum and dura mater were removed prior to testing, there is no energy absorption by these softer tissues and therefore the maximum force would be expected to be higher than that experienced in a real head impact. On the other hand, the cerebrospinal fluid and brain are also absent in this experimental protocol and thus not providing support to the cranial bones, presumably resulting in smaller maximum force magnitudes. In real-world impacts, the deformation pattern and force versus time curve may differ due to the stiffness and shape of the impacting surface and the soft tissue layers covering the skull.

Energy Absorbed to Failure

Margulies, Thibault [13] presented energy absorbed to failure data for their three-point bend tests under static loading conditions. For their six-month-old samples, the energy absorbed to failure was approximately 0.10 – 0.20 mJ/mm^3 and 0.40 – 0.45 mJ/mm^3 for loading rates of 2.54 and 2540 mm/min respectively. For a similar age group in the present study, specimens #1 and #2 had energy absorbed to failure of approximately 0.11 and 0.35 mJ/mm^3 indicating that energy absorbed to failure is similar for static and dynamic loading conditions at least in this age group.

Energy absorbed to failure increased with increasing age and hence average thickness. The data from all bone locations show this same general trend, with occipital bone having a much greater energy absorbing capacity than the others.

Implications for Finite Element Models

It is already known that bone behaviour is rate (velocity) sensitive and becomes more brittle elastic increasing strain rates [28]. The results of McPherson, Kriewall [14],Margulies, Thibault [13],Coats, Margulies [17],Davis et al. [16] show that infant and child cranial bone can exhibit noticeable elastic or plastic deformation without failure at low impact speeds (equivalent to falls less than one metre), while this study has shown that cranial bone exhibits prompt brittle fracture at relatively higher impact speeds (equivalent to falls of 1.6 m). Therefore, finite element models used for modelling head impacts in children need a suitable rate-dependent model for the cranial bone. The data presented here will help to verify predictions based on such models. There is also a future research question in that what strain rate or impact speed does the 'transition' from more compliant to relatively less compliant behaviour occur? Having a quantifiable value on this would help an analyst ensure that they are using a suitable material model that will account for the different behaviour of the cranial bone, especially for models of young children and teenagers.

Conclusions

The questions of current debate in the identification of AHT in children may be divided into the forensic (what injuries or injury patterns discriminate between AHT and accidental injury) and the mechanical (what are the elastic moduli, ultimate tensile strength and energy absorbed to failure of each of the head tissues, and how do they vary with strain rate and age). The results of the present study address a few of the latter:

- The failure mode in impacts of a 2 mm radius impactor at 5.65 ± 0.14 ms^{-1} was brittle fracture (with little or no bending observed) for samples aged two to 18 years. For the two specimens aged three-weeks, bending (resulting in inverted curvature of the specimens) occurred, followed by brittle fracture.
- Impact force peaks at 200 to 6000 N, increasing with age (or thickness). Impact force is higher for occipital than parietal or frontal bone.
- The energy absorbed to failure follows the same trend of increase with age or thickness. It was highest for occipital bone. The values of energy absorbed to failure were 0.11 and 0.35 mJ/mm^3 for age three-weeks, agreeing with previously published static tests, and increase with age up to around 9 mJ/mm^3 for 18-year-old occipital bone.
- The increase in stiffness with age and the differences in mechanical properties of the different cranial bones as seen by others is supported by the present data.
- The use of this data in FE modelling will contribute to answering the mechanical as well as the forensic questions in the identification of AHT.

The sample size is small, but the observations of the impact failure process, and the measurements of impact force and energy absorbed to failure are unique. To the best of the authors' knowledge, no data has yet been published for child specimens at this high loading rate; the highest speed in prior studies being 2.81 ms^{-1}.

References

1. Johnson K, Fischer T, Chapman S, Wilson B (2005) Accidental head injuries in children under 5 years of age. Clinical Radiology 60 (4):464-468. doi:10.1016/j.crad.2004.09.013

2. Plunkett J (2001) Fatal pediatric head injuries caused by short-distance falls. The American journal of forensic medicine and pathology 22 (1):1-12

3. Chadwick DL, Chin S, Salerno C, Landsverk J, Kitchen L (1991) DEATHS FROM FALLS IN CHILDREN - HOW FAR IS FATAL. JOURNAL OF TRAUMA-INJURY INFECTION AND CRITICAL CARE 31 (10):1353-1355

4. Hobbs CJ (1984) Skull fracture and the diagnosis of abuse. Archives of Disease in Childhood 59 (3):246-252. doi:10.1136/adc.59.3.246

5. Wilkins B (1997) Head injury—abuse or accident? Archives of disease in childhood 76 (5):393-397

6. Reece RM, Sege R (2000) Childhood head injuries: Accidental or inflicted? Archives of Pediatrics and Adolescent Medicine 154 (1):11-15

7. Roach JP, Acker SN, Bensard DD, Sirotnak AP, Karrer FM, Partrick DA (2014) Head injury pattern in children can help differentiate accidental from non-accidental trauma. Pediatric Surgery International 30 (11):1103-1106. doi:10.1007/s00383-014-3598-3

8. Williams R (1991) Injuries in infants and small children resulting from witnessed and corroborated free falls. Journal of Trauma and Acute Care Surgery 31 (10):1350-1352

9. Loyd AM (2011) Studies of the human head from neonate to adult: an inertial, geometrical and structural analysis with comparisons to the ATD head. Citeseer,

10. Hajiaghamemar M, Lan IS, Christian CW, Coats B, Margulies SS (2018) Infant skull fracture risk for low height falls. International journal of legal medicine:1-16

11. Li X, Sandler H, Kleiven S (2019) Infant skull fractures: Accident or abuse?: Evidences from biomechanical analysis using finite element head models. Forensic science international 294:173-182

12. Burgos-Flórez F, Garzón-Alvarado DA (2020) Stress and strain propagation on infant skull from impact loads during falls: a finite element analysis. International Biomechanics 7 (1):19-34

13. Margulies SS, Thibault KL (2000) Infant skull and suture properties: Measurements and implications for mechanisms of pediatric brain injury. Journal of Biomechanical Engineering 122 (4):364-371. doi:10.1115/1.1287160

14. McPherson GK, Kriewall TJ (1980) The elastic modulus of fetal cranial bone: a first step towards an understanding of the biomechanics of fetal head molding. Journal of biomechanics 13 (1):9-16

15. Wang J, Zou D, Li Z, Huang P, Li D, Shao Y, Wang H, Chen Y (2014) Mechanical properties of cranial bones and sutures in 1–2-year-old infants. Medical science monitor: international medical journal of experimental and clinical research 20:1808

16. Davis MT, Loyd AM, Shen H-yH, Mulroy MH, Nightingale RW, Myers BS, Bass CD (2012) The mechanical and morphological properties of 6 year-old cranial bone. Journal of Biomechanics 45 (15):2493-2498. doi:10.1016/j.jbiomech.2012.07.001

17. Coats B, Margulies SS (2006) Material properties of human infant skull and suture at high rates. Journal of Neurotrauma 23 (8):1222-1232. doi:10.1089/neu.2006.23.1222

18. Brooks T, Choi JE, Garnich M, Hammer N, Waddell JN, Duncan W, Jermy M (2018) Finite element models and material data for analysis of infant head impacts. Heliyon 4 (12):e01010

19. Ommaya A, Goldsmith W, Thibault L (2002) Biomechanics and neuropathology of adult and paediatric head injury. British journal of neurosurgery 16 (3):220-242

20. Anjomrouz M (2017) Investigation of MARS spectral CT: X-ray source and detector characterization. University of Otago,

21. Bateman CJ (2015) Methods for material discrimination in MARS multi-energy CT. University of Otago,

22. Matanaghi A, Raja A, Leary C, Amma MR, Panta R, Anjomrouz M, Moghiseh M, Butler A, Bamford B, Collaboration M (2019) Semi-automatic quantitative assessment of site-specific bone health using spectral photon counting CT. Journal of Nuclear Medicine 60 (supplement 1):1297-1297

23. Schneider CA, Rasband WS, Eliceiri KW (2012) NIH Image to ImageJ: 25 years of image analysis. Nature methods 9 (7):671-675

24. Schindelin J, Arganda-Carreras I, Frise E, Kaynig V, Longair M, Pietzsch T, Preibisch S, Rueden C, Saalfeld S, Schmid B (2012) Fiji: an open-source platform for biological-image analysis. Nature methods 9 (7):676

25. Photron (2019) Photron FASTCAM Viewer. 4.0.2.2 edn.,

26. Baumer TG, Passalacqua NV, Powell BJ, Newberry WN, Fenton TW, Haut RC (2010) Age-dependent fracture characteristics of rigid and compliant surface impacts on the infant skull—a porcine model. Journal of forensic sciences 55 (4):993-997

27. Loyd AM, Nightingale RW, Luck JF, Song Y, Fronheiser L, Cutcliffe H, Myers BS, Bass CRD (2015) The compressive stiffness of human pediatric heads. Journal of biomechanics 48 (14):3766-3775

28. Kieser J (2012) Biomechanics of Bone and Bony Trauma. In: Kieser J, Taylor M, Carr DD (eds) Forensic biomechanics. vol Book, Whole. Wiley-Blackwell, Chichester, West Sussex, UK,

29. Delye H, Clijmans T, Mommaerts MY, Sloten JV, Goffin J (2015) Creating a normative database of age-specific 3D geometrical data, bone density, and bone thickness of the developing skull: a pilot study. Journal of Neurosurgery: Pediatrics 16 (6):687-702

Tables

Table 1 Human specimen information

Specimen #	Age (Years)	Sex	Cranial Bone	Span (mm)	Width (mm)	Thickness (mm)
1	3 weeks	Male	Occipital	20.5	11.4	1.1
2	3 weeks	Male	Parietal	20.7	9.5	1.0
3	2	Male	Frontal	14.7	9.5	2.1
4	4	Male	Frontal	16.5	10.0	3.2
5	4	Male	Parietal	22.4	10.8	3.7
6	12	Female	Frontal	18.7	9.9	5.0
7	13	Female	Occipital	16.4	10.8	6.1
8	13	Female	Parietal	15.3	9.6	4.8
9	17	Male	Frontal	15.6	10.4	5.6
10	17	Male	Temporal	18.2	10.1	6.2
11	18	Female	Occipital	15.2	7.7	6.7

All measurements have error of ± 0.1 mm

Table 2 Camera settings

Setting	
Frame Rate (s^{-1})	20 000
Shutter Speed (s)	1.09E-05
Resolution (pixels)	704x520

Figures

Fig. 1 Specimens mounted in 3D printed capsule (cover removed) for CT scanning

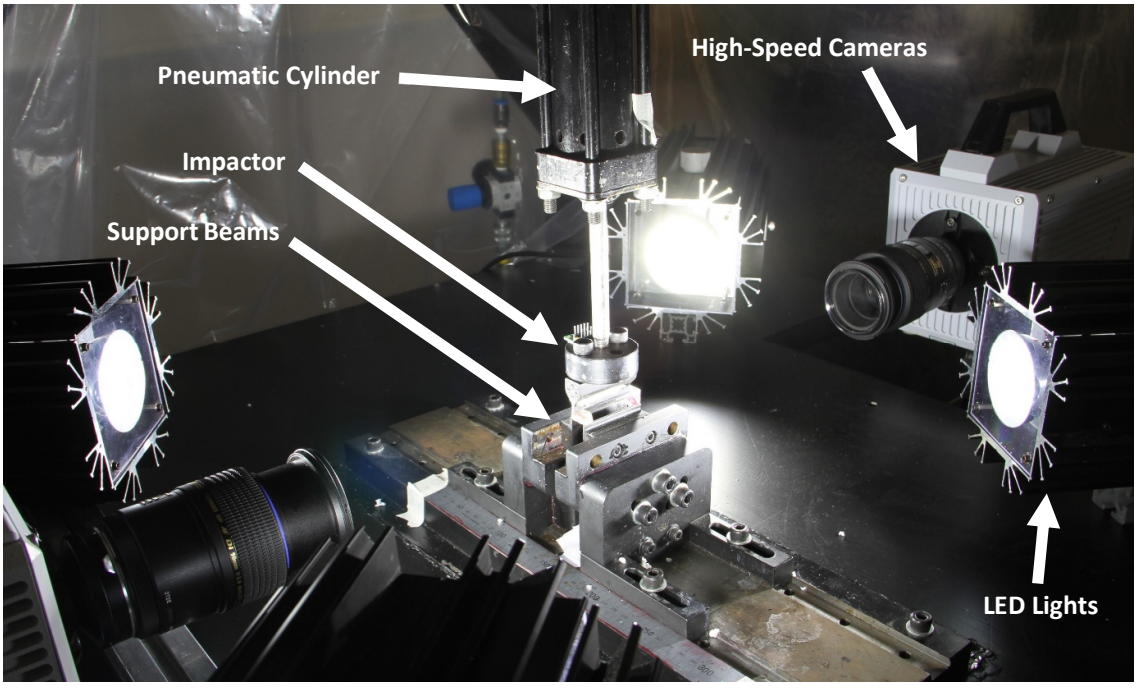

Fig. 2 Impact test machine, including high-speed camera and pneumatic cylinder

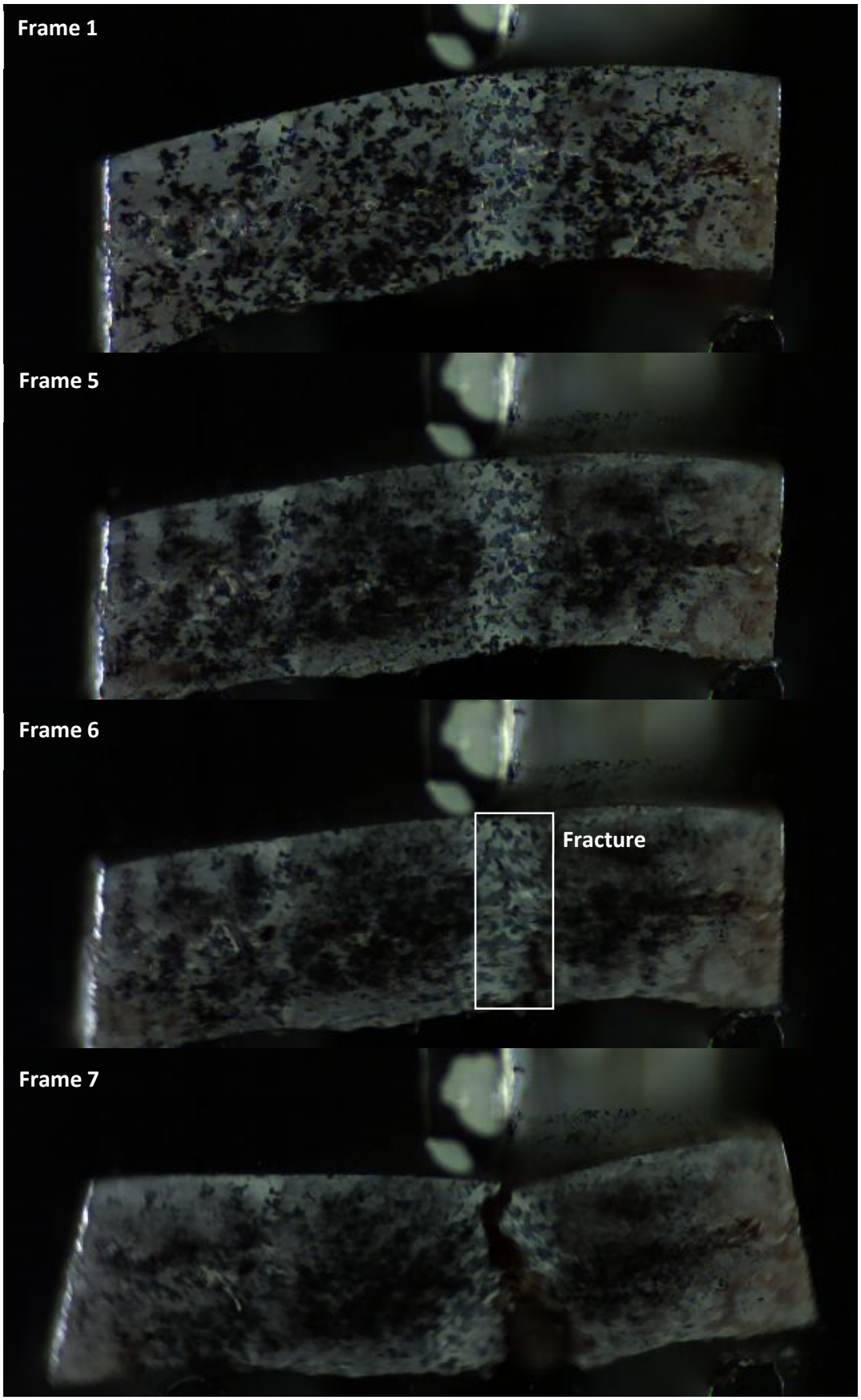

1

Fig. 3 High-speed imagery sequence for specimen #6. Frame 1 (F1) is just before impact; impactor has speed of 5.75 ± 0.33 ms^{-1}. During F2-F4 (not shown), the specimen 'settles' onto the support beams. In F5, internal compression in cancellous layer occurs. Fracture appears in F6 (boxed outline); initiates at the bottom. In F7, the specimen is broken into two pieces.

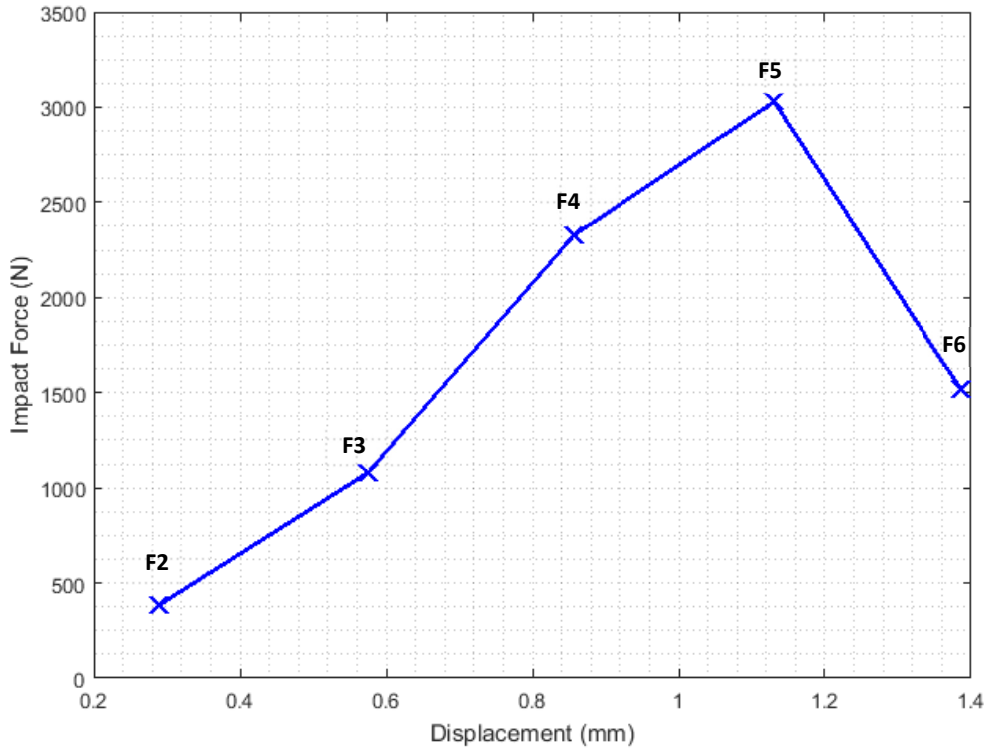

Fig. 4 Force-displacement plot for specimen six. Data points correspond to frames two (F2) through to six (F6)

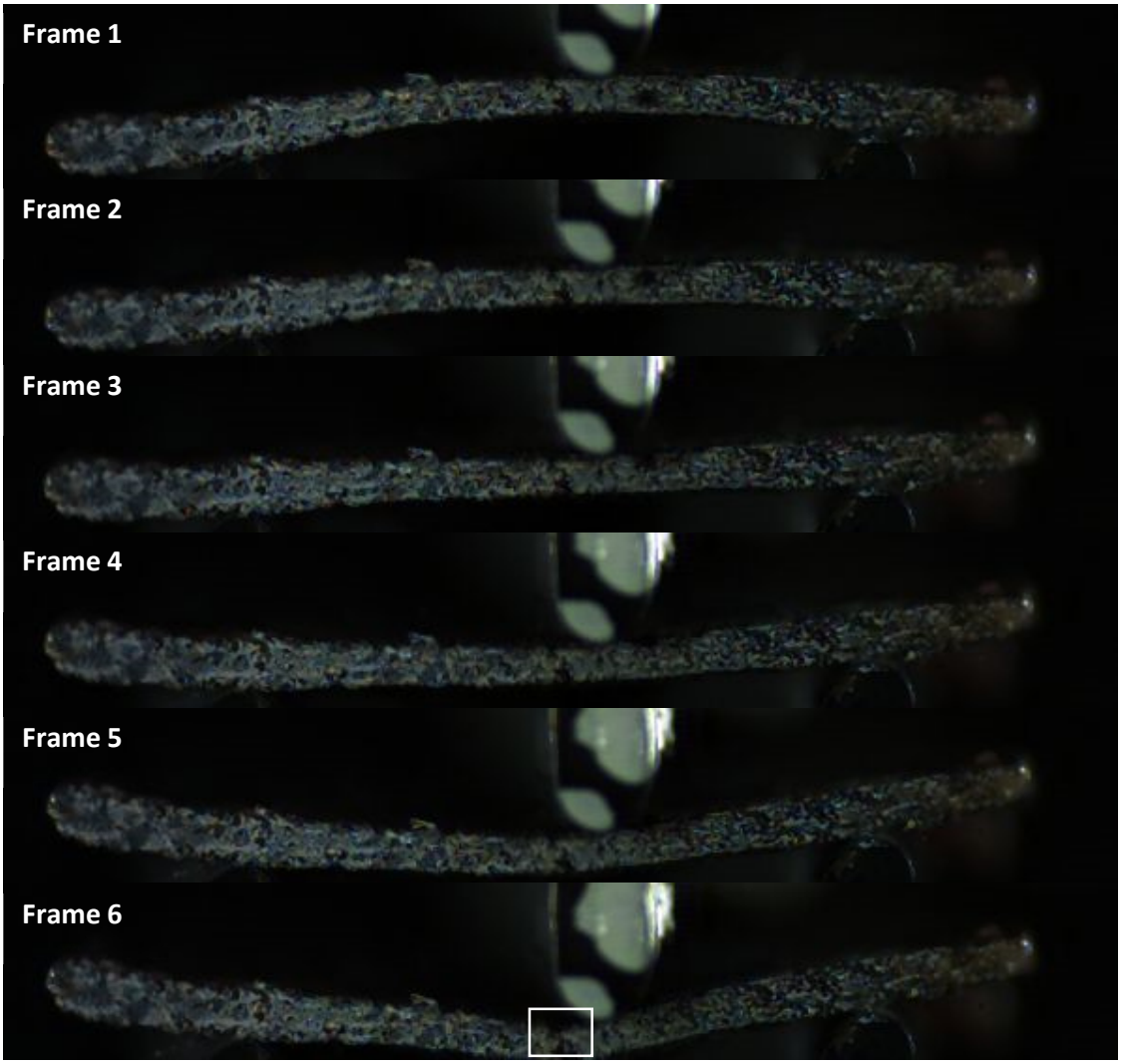

Fig. 5 Sequence of events for specimen #2. Frame 1 (F1) is just before the impact; the impactor has a speed of 5.80 ± 0.34 ms^{-1} and the specimen is concave down. From F2 to F5, bending occurs. In F6, fracture occurs (boxed outline).

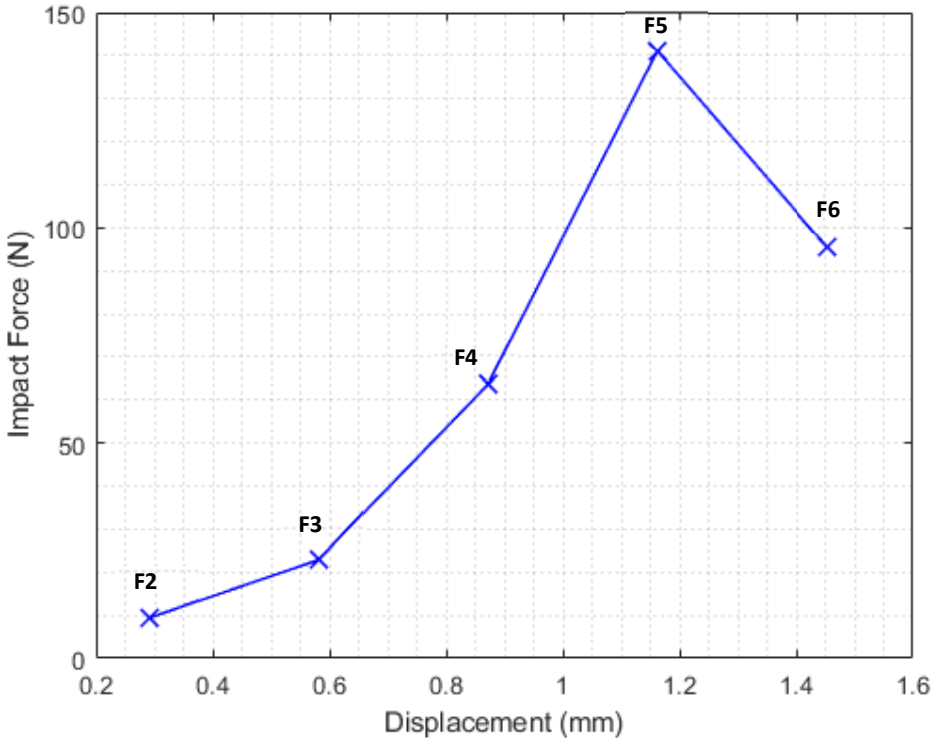

Fig. 6 Force-displacement plot for specimen two. Data points correspond to frames two (F2) through to six (F6)

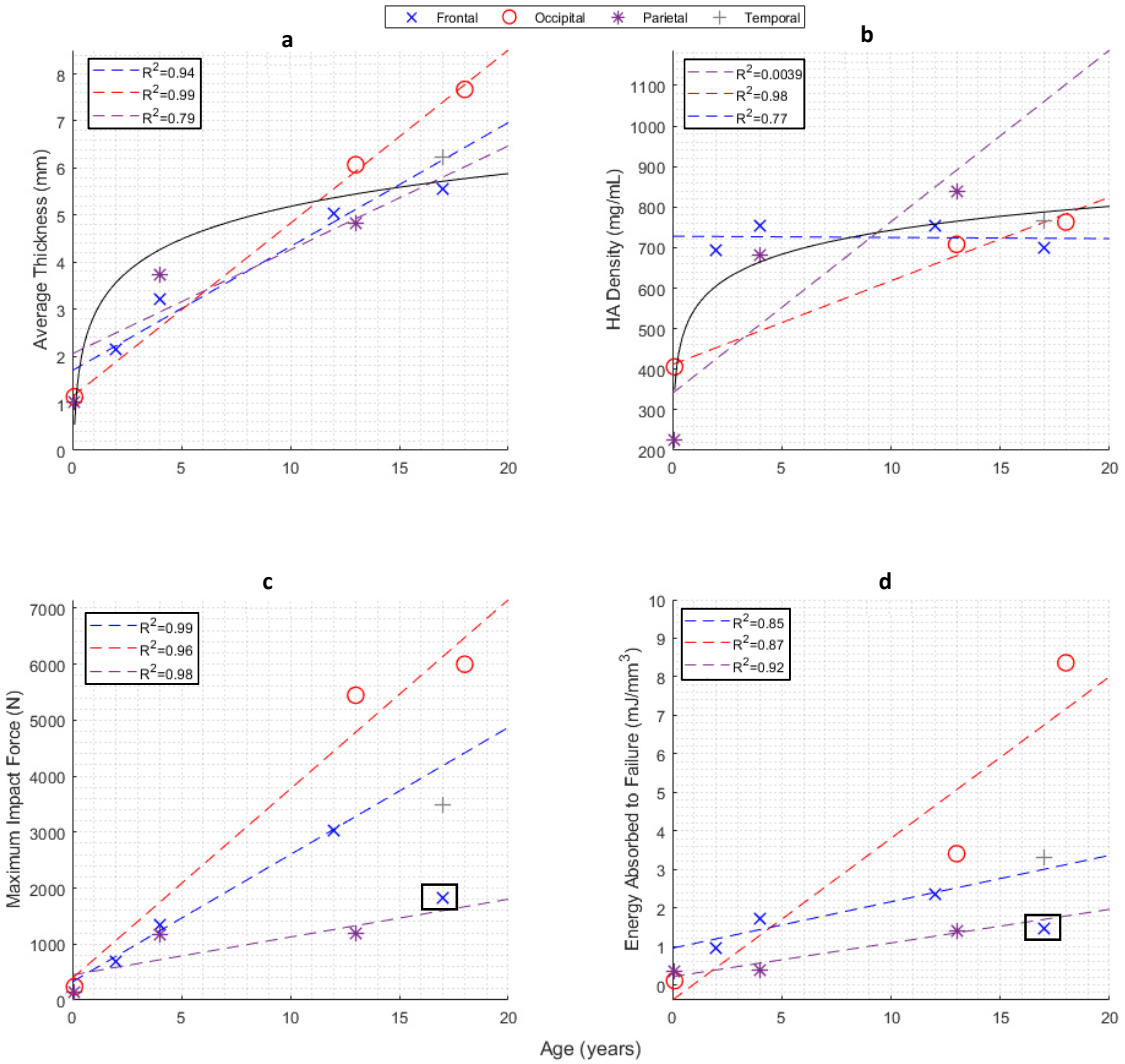

Fig. 7 Plots of average thickness (**a**), HA density (**b**), maximum impact force (**c**) and energy absorbed to failure (**d**) versus age. Dashed regression lines correspond to respective cranial bone data by colour. Solid black curves correspond to logarithmic fit (used in pre-existing literature) for all data points. Boxed data points in (**c**) and (**d**) signify outliers and were not used in the regression analysis. Uncertainties are ± 0.02 mm, ± 5.8% and ± 12% for average thickness, maximum impactor force and energy absorbed to failure respectively; (**c**) and (**d**) are presented with these uncertainties in the Appendix for clarity (Fig 8 and 9).

Appendix

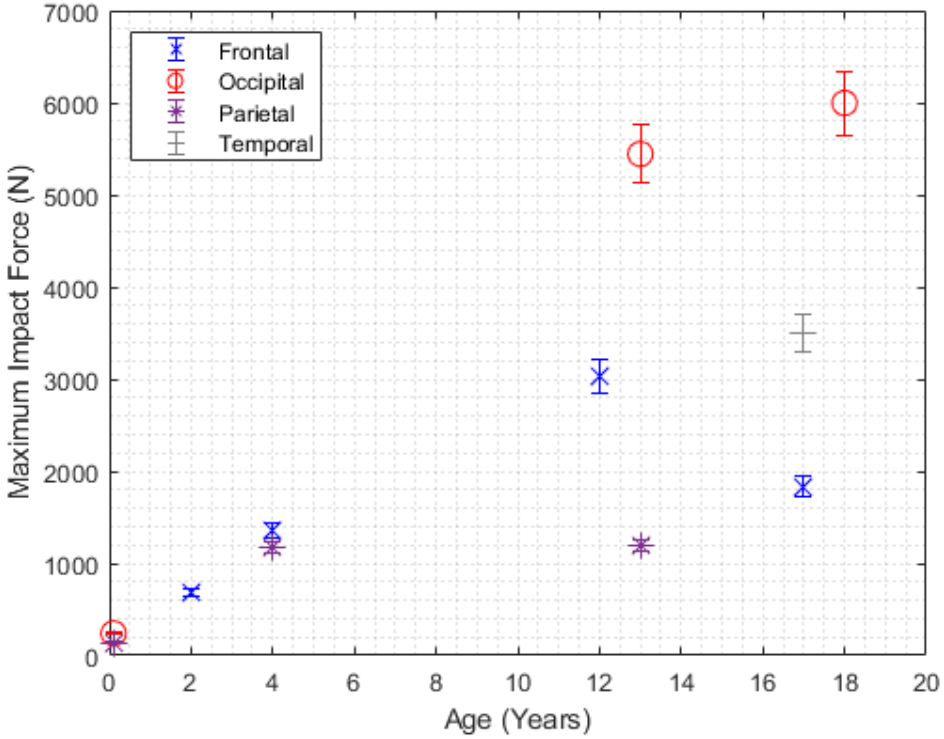

Fig. 8 Maximum impact force versus age (with uncertainties)

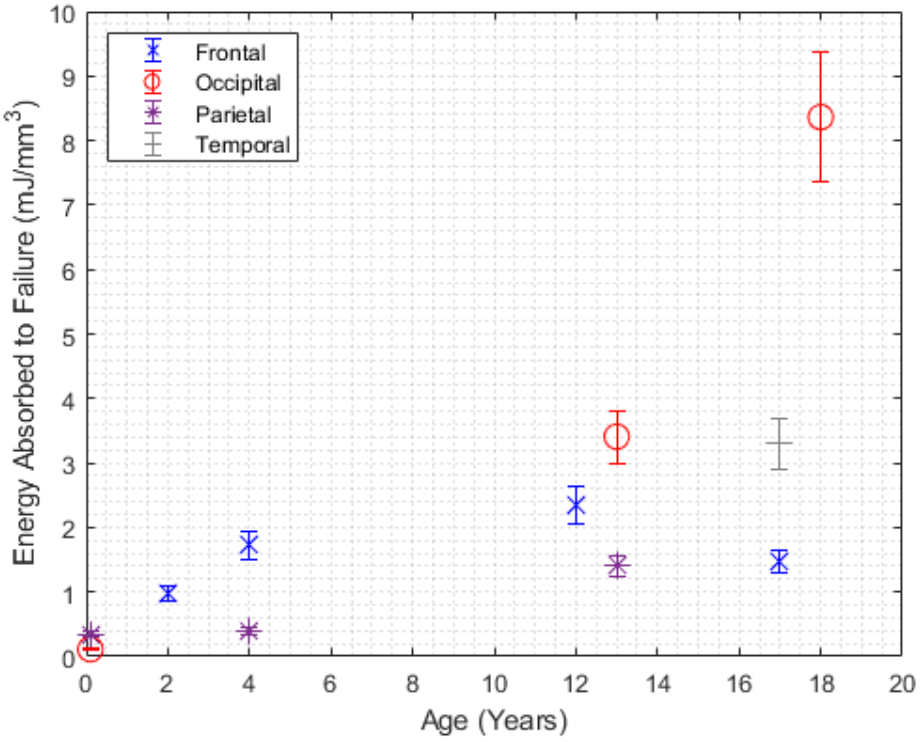

Fig. 9 Energy absorbed to failure versus age (with uncertainties)